Monthly Notices
of the
ROYAL ASTRONOMICAL SOCIETY

MNRAS **456,** 270–277 (2016) doi:10.1093/mnras/stv2655

Role of the H_2^+ channel in the primordial star formation under strong radiation field and the critical intensity for the supermassive star formation

K. Sugimura,[1]★ C. M. Coppola,[2,3] K. Omukai,[1] D. Galli[3] and F. Palla[3]

[1]*Astronomical Institute, Tohoku University, Aoba, Sendai 980-8578, Japan*
[2]*Dipartimento di Chimica, Università degli Studi di Bari, Via Orabona 4, I-70126 Bari, Italy*
[3]*INAF-Osservatorio Astrofisico di Arcetri, Largo E. Fermi 5, I-50125 Firenze, Italy*

Accepted 2015 November 9. Received 2015 October 27; in original form 2015 September 15

ABSTRACT

We investigate the role of the H_2^+ channel on H_2 molecule formation during the collapse of primordial gas clouds immersed in strong radiation fields which are assumed to have the shape of a diluted blackbody spectra with temperature $T_{\rm rad}$. Since the photodissociation rate of H_2^+ depends on its level population, we take full account of the vibrationally resolved H_2^+ kinetics. We find that in clouds under soft but intense radiation fields with spectral temperature $T_{\rm rad} \lesssim 7000\,{\rm K}$, the H_2^+ channel is the dominant H_2 formation process. On the other hand, for harder spectra with $T_{\rm rad} \gtrsim 7000\,{\rm K}$, the H^- channel takes over H_2^+ in the production of molecular hydrogen. We calculate the critical radiation intensity needed for supermassive star formation by direct collapse and examine its dependence on the H_2^+ level population. Under the assumption of local thermodynamic equilibrium (LTE) level population, the critical intensity is underestimated by a factor of a few for soft spectra with $T_{\rm rad} \lesssim 7000\,{\rm K}$. For harder spectra, the value of the critical intensity is not affected by the level population of H_2^+. This result justifies previous estimates of the critical intensity assuming LTE populations since radiation sources like young and/or metal-poor galaxies are predicted to have rather hard spectra.

Key words: molecular processes – quasars: supermassive black holes – cosmology: theory.

1 INTRODUCTION

The collapse of primordial gas clouds can lead to the formation of ordinarily massive stars (10–100 $M_\odot$, hereafter Pop III stars; see, e.g. Yoshida, Omukai & Hernquist 2008; Hosokawa et al. 2011) or supermassive stars ($M \gtrsim 10^5\,M_\odot$, hereafter SMS; see, e.g. Bromm & Loeb 2003), depending on the strength of the radiation fields in the ambient medium. Pop III stars form by H_2 cooling in the absence of a strong Lyman–Werner (LW) radiation field ($h\nu = 11.2$–$13.6\,{\rm eV}$). Conversely, in a cloud irradiated by an extremely strong LW radiation field, H_2 is completely destroyed, and cooling is suppressed. In the latter case, if the cloud is in a halo with virial temperature higher than $\sim 10^4\,{\rm K}$, it can still collapse via atomic cooling (Omukai 2001), without experiencing major episodes of fragmentation (Bromm & Loeb 2003; Regan & Haehnelt 2009a,b; Inayoshi, Omukai & Tasker 2014; Latif et al. 2014; Regan, Johansson & Haehnelt 2014a; Regan, Johansson & Wise 2014b; Becerra et al. 2015; Choi, Shlosman & Begelman 2015), and an embryonic protostar can grow rapidly to an SMS by subsequent accretion (Hosokawa, Omukai & Yorke 2012; Hosokawa et al. 2013; Sakurai et al. 2015; Shlosman et al. 2015). The latter eventually collapses due to the post-Newtonian instability, leaving a black hole with $\sim 10^5\,M_\odot$ (see, e.g. Shapiro & Teukolsky 1983). This process, called 'direct', or 'monolithic' collapse, leads to the formation of SMS remnants that are promising candidates for being the seeds of the supermassive ($\gtrsim 10^9\,M_\odot$) black holes (SMBHs) observed at redshift $z \gtrsim 6$ (see, e.g. Fan et al. 2001; Mortlock et al. 2011; Venemans et al. 2013; Wu et al. 2015).

The feasibility of this scenario can be tested by comparing the observed number density of the high-z SMBHs $n_{\rm SMBH}$ with the theoretical predictions. By considering the probability distribution of the LW intensity J_{21} around haloes,[1] $n_{\rm SMBH}$ can be estimated from the critical value of LW intensity $J_{21}^{\rm cr}$ needed for the formation of SMS (Dijkstra et al. 2008; Agarwal et al. 2012; Dijkstra, Ferrara & Mesinger 2014; Inayoshi & Tanaka 2015). Sugimura et al. (2014, hereafter SOI14) found $J_{21}^{\rm cr} \sim 1000$ for realistic young-galaxy spectra. Combined with the J_{21} probability distribution by Dijkstra

[1] We use the specific intensity at the centre of the LW bands, $J_{21} \equiv J_\nu(h\nu = 12.4\,{\rm eV})/10^{-21}\,{\rm erg\,s^{-1}\,cm^{-2}\,Hz^{-1}\,sr^{-1}}$ to quantify the intensity of external radiation.

★ E-mail: sugimura@astr.tohoku.ac.jp

et al. (2014), this gives $n_{\rm SMBH} \sim 10^{-10}\,{\rm Mpc}^{-3}$, in rough agreement with the observed values. However, the predicted $n_{\rm SMBH}$ is still uncertain due to our poor knowledge of $J_{21}^{\rm cr}$ from insufficient modelling of the physical/chemical processes in primordial gas clouds (see, e.g. Glover 2015a,b), and of the nature of the high-redshift sources responsible for this radiation.

In the low-density primordial gas ($\lesssim 10^8\,{\rm cm}^{-3}$), H_2, the main coolant in the low temperatures regime, is formed either via the H^- channel or via the H_2^+ channel. The former begins with the formation of H^- by radiative attachment,

$$H + e \rightarrow H^- + \gamma, \quad (1)$$

followed by H_2 formation by associative detachment

$$H^- + H \rightarrow H_2 + e. \quad (2)$$

Similarly, the H_2^+ channel starts with H_2^+ formation by radiative association

$$H + H^+ \rightarrow H_2^+ + \gamma, \quad (3)$$

followed by the charge transfer reaction

$$H_2^+ + H \rightarrow H_2 + H^+. \quad (4)$$

In each channel, the second step proceeds much faster than the first one and its rate determines the amount of H_2 formation. Since the rate coefficient for reaction (1) ($k_{\rm ra}^{\rm H^-} \sim 6 \times 10^{-15}\,{\rm cm^3\,s^{-1}}$ at 8000 K; Galli & Palla 1998, hereafter GP98) is about one order of magnitude larger than that for reaction (3) ($k_{\rm ra}^{\rm H_2^+} \sim 1.5 \times 10^{-16}\,{\rm cm^3\,s^{-1}}$ at 8000 K; GP98), the H^- channel is usually much more efficient than that involving H_2^+. However, under a strong radiation field, both channels become irrelevant due to the destruction of the intermediaries by the H^- photodetachment

$$H^- + \gamma \rightarrow H + e, \quad (5)$$

and H_2^+ photodissociation

$$H_2^+ + \gamma \rightarrow H + H^+. \quad (6)$$

Since the binding energy of H^- (0.76 eV) is smaller than that of H_2^+ (2.7 eV for the ground state), H^- is photodestroyed more easily than H_2^+ and reaction (4) can become the dominant source of H_2 in the primordial gas.

Here, it should be noted that the H_2^+ photodissociation rate depends sensitively on the internal level population, because H_2^+ in high vibrational levels is much more vulnerable to photodissociation. As an example, the binding energy of H_2^+ in vibrational levels $v = 6$ and 18 is only 1.2 and 0.003 eV, respectively. Thus, the level population of H_2^+ is determined by a complex interplay of reactions, involving formation (reaction 3), collisional dissociation (reaction 4), photodissociation (reaction 6), collisional excitation/de-excitation and radiative de-excitation. Therefore, in order to accurately implement the effects of the H_2^+ channel, a detailed calculation of its level population is needed.

In the post-recombination era, H_2 formation is primarily controlled by the H_2^+ channel for redshift $z > 100$, owing to the suppression of H^- by the cosmic microwave background (CMB) radiation (see, e.g. GP98). However, the efficiency of the H_2^+ channel depends strongly on its level population: if H_2^+ is in the ground state, the H_2^+ channel is so efficient as to produce most of the H_2 molecules at a level $y(H_2) \sim 10^{-4}$. On the other hand, under local thermodynamic equilibrium (LTE), the H_2^+ channel makes only a minor contribution to H_2, whose final abundance remains limited to $y(H_2) \sim 10^{-6}$. Recently, Hirata & Padmanabhan (2006), Coppola et al. (2011, hereafter C11) and Longo et al. (2011) have studied the chemistry of the early Universe computing the population of the vibrational levels of H_2 and H_2^+ following a state-to-state reaction kinetics, and found that H_2^+ forms by reaction (3) preferentially in excited states. As a result, H_2^+ channel does not dominate the formation of H_2, and the final H_2 abundance is limited by H^- at a level $y(H_2) \sim 10^{-6}$.

Although the efficiency of the H_2^+ channel depends strongly on the H_2^+ level population, the LTE rate (Stancil 1994; Mihajlov et al. 2007) has been widely used in studying primordial gas clouds without a real justification. An exception is Glover (2015a) who calculated $J_{21}^{\rm cr}$ for blackbody-type spectra with temperatures $T_{\rm rad} = 10^4$ and 10^5 K under two assumptions for the H_2^+ level population: (i) all the H_2^+ is in the vibrational ground state, and (ii) all levels are in LTE. Although the difference in $J_{21}^{\rm cr}$ in the two cases is not significant, it is not yet clear in what circumstances and to what extent the H_2^+ channel can affect the evolution of primordial gas clouds.

In this paper, we compute the thermal and chemical evolution of primordial gas clouds under a strong external radiation field with J_{21} around $J_{21}^{\rm cr}$ by computing the H_2^+ vibrational level population, and assess the effect of H_2 formation via the H_2^+ channel. We also determine the critical intensity for SMS formation and examine its dependence on the H_2^+ level population by comparing our non-LTE results to those obtained in the LTE or ground state approximations.

The paper is organized as follows. In Section 2, we describe our model for collapsing primordial gas clouds. In Section 3, we present the result of our calculation. The implications and conclusions are described Section 4.

2 MODEL

2.1 Basic equations

To follow the gravitational collapse of primordial gas clouds, we use the one-zone model described in SOI14 (see also Omukai 2001), updated as follows: the vibrational level population of H_2^+ is resolved following C11; a part of the chemical network is updated following Glover (2015a,b). In our model, we compute physical quantities in the homogeneous central part of the self-similar solution of collapsing clouds (Larson 1969; Penston 1969; Yahil 1983). The qualitative validity of the one-zone model has been confirmed recently by three-dimensional hydrodynamical simulations (Shang, Bryan & Haiman 2010; Latif et al. 2014). Thanks to the substantial simplification of gas dynamics, we can focus on the thermo-chemical processes in detail.

According to the one-zone model, the evolution of the gas density ρ is modelled as

$$\frac{{\rm d}\rho}{{\rm d}t} = \frac{\rho}{t_{\rm ff}}, \quad (7)$$

where $t_{\rm ff} = \sqrt{3\pi/32G(\rho + \rho_{\rm DM})}$ is the free-fall time, G is the gravitational constant and $\rho_{\rm DM}$ is the dark matter density, which is assumed to evolve following the solution of the spherical top-hat collapse model until it reaches the virial density. The radius of the core is approximately given by the Jeans length $\lambda_{\rm J} = \sqrt{\pi k T_{\rm gas}/G\rho\mu m_{\rm p}}$, where $m_{\rm p}$ is the proton mass, μ is the mean molecular weight and k is the Boltzmann constant. The evolution of the gas temperature $T_{\rm gas}$ is determined by the energy equation,

$$\frac{{\rm d}e_{\rm kin}}{{\rm d}t} = \Gamma_{\rm c} - \Lambda_{\rm rad} - \frac{{\rm d}e_{\rm int}}{{\rm d}t}, \quad (8)$$

where $e_{\rm kin} = 3k\,T_{\rm gas}/2\mu\,m_{\rm p}$ is the kinetic energy of the gas per unit mass, $\Gamma_{\rm c} = (\rho\,k\,T_{\rm gas}/\mu\,m_{\rm p})\,({\rm d}/{\rm d}t)\,(1/\rho)$ the compressional heating rate, $\Lambda_{\rm rad}$ the net cooling/heating rate due to radiative processes and $e_{\rm int}$ the internal energy of the gas per unit mass, including both chemical energy and internal molecular energy. In the density and temperature range of our interest, the dominant cooling processes are H_2 (Glover & Abel 2008), updated according to Glover (2015a), and Ly α emission (Anninos et al. 1997). Other radiative reactions or the time variation of $e_{\rm int}$ hardly affect the evolution of $T_{\rm gas}$.

We model the external radiation field as a diluted blackbody with cut-off energy at 13.6 eV, specifying its temperature $T_{\rm rad}$ and intensity J_{21} at 12.4 eV. We limit our analysis to blackbody spectra with various $T_{\rm rad}$ although realistic spectra of galaxies are more complex and not well represented by a blackbody spectrum (SOI14, Agarwal & Khochfar 2015). SOI14 claimed that the ratio of the H^- photodetachment rate to the H_2 photodissociation rate, $k_{\rm pd}^{\rm H^-}/k_{\rm pd}^{\rm H_2}$, is a key parameter characterizing the hardness of the spectra, and that typical young and/or metal-poor galaxies have hard spectra with $k_{\rm pd}^{\rm H^-}/k_{\rm pd}^{\rm H_2} \lesssim 10^3$, corresponding to blackbody spectra with $T_{\rm rad} \gtrsim 2 \times 10^4$ K. None the less, we explore a broad range of blackbody temperatures, $T_{\rm rad} > 5 \times 10^3$ K, to mimic the evolution in a variety of environments possibly present in the early Universe.

2.2 Chemistry

In this section, we review our vibrationally resolved chemical network based on SOI14 and C11. We consider 29 chemical species (H, H^+, H^-, H_2, $H_2^+(v)$ with $v = 0, 1 \ldots, 18$, He, He^+, He^{2+}, HeH^+, H_3^+ and e), and we compute the evolution of the fractional abundance of species i, $y(i) \equiv n(i)/n_{\rm H}$, where $n(i)$ is the number density of species i and $n_{\rm H}$ the number density of hydrogen nuclei. We do not consider deuterium chemistry because it should only affect the evolution of the gas with $T_{\rm gas}$ below a few hundred kelvin by HD cooling, a temperature regime that is never attained in our calculations (see, e.g. Nagakura & Omukai 2005; McGreer & Bryan 2008; Wolcott-Green & Haiman 2011; Nakauchi, Inayoshi & Omukai 2014).

The processes involving H_2^+ are the following. The vibrationally resolved reactions in our code are H_2^+ formation by radiative association (reaction 3), H_2^+ photodissociation (reaction 6), H_2^+ dissociation by charge transfer (reaction 4), vibrational excitation/de-excitation by collision with H and vibrational de-excitation by spontaneous emission. We do not resolve rotational levels of H_2^+, because the dependence of the efficiency of H_2^+ photodissociation on rotational levels is weaker than on vibrational levels (Dunn 1968; Babb 2015). In addition, complete rovibrational state-resolved data are not available in the literature. Note that H_2^+ formation via HeH^+ hardly affects the evolution of primordial clouds (see, however, GP98 or C11 for its consequences on the chemistry of the early Universe).

The state-resolved data adopted in our chemical network are the following. Babb (2015) provides rovibrationally resolved data for radiative association and H_2^+ photodissociation, which are summed up with respect to rotational levels to obtain the vibrationally resolved rate coefficients. To obtain vibrationally resolved H_2^+ photodissociation rate we assume rotational level population as explained in Appendix A. Fig. 1 shows the H_2^+ photodissociation rates $k_{\rm pd}^{\rm H_2^+}$ for a blackbody radiation field and $J_{21} = 1$, obtained assuming (rovibrational) LTE population with $T_{\rm rad} = 1000$, 3000 and 8000 K, and all H_2^+ in the ground state. Fig. 1 clearly shows that H_2^+ becomes more easily photodissociated as the H_2^+ vibrational state becomes more excited. Krstić's data base (Krstić, Schultz & Janev 2002; Krstić 2005; Krstic & Schultz 1999; Krstić, Schultz & Janev 2002; Krstić & Janev 2003) provides vibrationally resolved data for charge transfer and vibrational excitation/de-excitation by collision with H. The rovibrationally resolved de-excitation rates of H_2^+ by spontaneous emission are taken from Posen, Dalgarno & Peek (1983) and summed up with respect to rotational levels to obtain the vibrationally resolved rates. Recently, Olivares Pilón & Baye (2012) have re-calculated the spontaneous emission rates for low vibrational states up to $v = 3$ with a very high accuracy of nine digits and confirmed that the results of Posen et al. (1983) agree with theirs with at most a few per cent difference. To see the dependence of the evolution of the clouds on the assumed H_2^+ level population, in addition to the standard state-resolved runs (hereafter non-LTE model), we also perform runs using the (rovibrational) LTE H_2^+ photodissociation rate (hereafter LTE model) and runs using the H_2^+ photodissociation rate for H_2^+ in the (rovibrational) ground state (hereafter ground-state model).

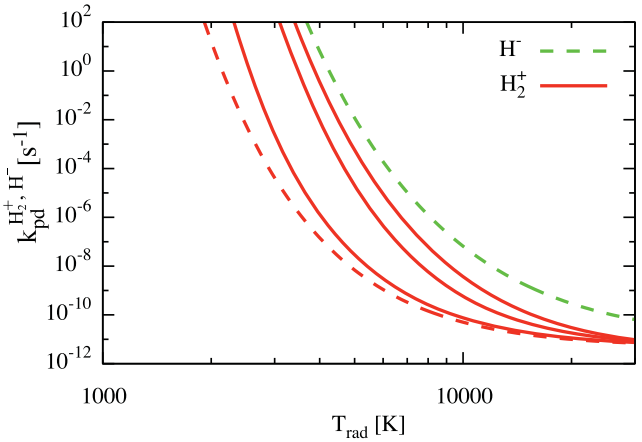

Figure 1. Photodissociation rate of H_2^+ from the ground vibrational state (dashed red curve) and assuming LTE level populations with $T_{\rm rad} = 1000$, 3000 and 8000 K (solid red curves, bottom to top). The dashed green curve shows the H^- photodetachment rate. The radiation spectrum is a diluted blackbody normalized as $J_{21} = 1$.

We review here our treatment of H^- photodetachment and indirect H_2 photodissociation (the so-called Solomon process). Fig. 1 shows the H^- photodetachment rate coefficient $k_{\rm pd}^{\rm H^-}$ for a blackbody radiation field normalized to $J_{21} = 1$ as a function of $T_{\rm rad}$. Here, the cross-section by John (1988), which is a fit to the results of Wishart (1979), is used. Although it has recently been updated by Miyake et al. (2010) to include the effects of some resonances at high photon energies ($\gtrsim$11 eV), we use the data by John (1988) as before, since their cross-section is just a few per cent larger for a blackbody radiation field with $T_{\rm rad} \lesssim 2 \times 10^4$ K, as considered in this paper. As seen in Fig. 1, the H^- photodetachment is generally more effective than H_2^+ photodissociation although the latter depends on the H_2^+ level population. For the H_2 photodissociation rate coefficient, we adopt the formula by Wolcott-Green, Haiman & Bryan (2011),

$$k_{\rm pd}^{\rm H_2} = 1.4 \times 10^{-12}\,f_{\rm sh}\,J_{21}\,{\rm s}^{-1}, \quad (9)$$

where $f_{\rm sh}$ is the self-shielding factor (for the explicit form, see equation 10 of Wolcott-Green et al. 2011). For the radiation spectra considered in Fig. 5, equation (9) gives $k_{\rm pd}^{\rm H_2} = 1.4 \times 10^{-12}\,{\rm s}^{-1}$ without self-shielding ($f_{\rm sh} = 1$). The fact that $k_{\rm pd}^{\rm H_2^+}$ and $k_{\rm pd}^{\rm H^-}$ are decreasing functions of $T_{\rm rad}$ can be understood as the photodissociation of H_2^+ and the photodetachment of H^- are relatively more effective for softer spectra, compared to the photodissociation of H_2. Note that

the exact form of f_{sh} is not settled in the literature (see, e.g. Draine & Bertoldi 1996; Wolcott-Green et al. 2011; Richings, Schaye & Oppenheimer 2014; Hartwig et al. 2015), which may introduce an uncertainty in the value of J_{21}^{cr} by a factor of a few, as pointed out in SOI14 and Glover (2015b). Similarly, evaluating $k_{pd}^{H_2}$ with the intensity at a single frequency $h\nu = 12.4$ eV, may introduce an uncertainty in the value of J_{21}^{cr} by a factor of a few if the spectrum changes substantially within the LW bands, as mentioned in SOI14. However, since the above uncertainties should not affect the conclusion of this paper, we leave these issues for future studies.

We updated the chemical network of SOI14, following Glover (2015a,b). We include dissociative tunnelling of H_2 to an unbound state (Martin, Schwarz & Mandy 1996) and H collisional ionization with H (Gealy & van Zyl 1987; Lenzuni, Chernoff & Salpeter 1991) and He (van Zyl, Le & Amme 1981; Lenzuni, Chernoff & Salpeter 1991). We replace the direct H_2 collisional dissociation rate with the fit given in Martin et al. (1996).

2.3 Initial conditions

Following Omukai, Schneider & Haiman (2008) and SOI14, we take as initial conditions of the calculation the following values corresponding to the turnaround redshift $z = 16$: $T_{gas} = 21$ K, $n_H = 4.5 \times 10^{-3}$ cm^{-3}, $y(e) = 3.7 \times 10^{-4}$, $y(He) = 8.3 \times 10^{-2}$, $y(H_2) = 2 \times 10^{-6}$ and $y(i) = 0$ for the other species. Note that the initial chemical composition hardly affects the thermal evolution of the clouds: at the beginning of the evolution well within the initial adiabatic contraction phase, most of pre-existing H_2 is photodissociated under a strong LW radiation field with J_{21} around J_{21}^{cr}; $y(e)$ settles to the value determined by the condition that the recombination time-scale is about the same as the dynamical (free-fall) one; and the abundances of the other species reach the values in chemical equilibrium (Omukai 2001).

3 RESULTS

In the following, we show how the temperature evolution of the cloud is modified by the assumed H_2^+ vibrational level population. Then, we calculate the critical intensity of the radiation field J_{21}^{cr} as a function of the blackbody temperature and assess the importance of H_2 formation via the H_2^+ channel on the evolution of the primordial clouds.

3.1 Thermal evolution of the cloud

The run of the temperature, chemical abundance and H_2^+ level populations of a cloud irradiated by a blackbody radiation field with $T_{rad} = 6000$ K and $J_{21} = 0.05$ as a function of the H number density are shown in Figs 2, 3 and 4, respectively. In Figs 2 and 3, we also plot for comparison purposes the results for the ground-state and LTE models, along with the fiducial results for the non-LTE model. In Fig. 4, instead, we also plot the LTE populations with the temperature given by T_{gas} in the non-LTE model (i.e. the solid red curve in Fig. 2) along with the results for the non-LTE model, because the difference in T_{gas} in the non-LTE and LTE models makes it difficult to extract the effect of non-LTE chemistry by directly comparing the populations in these models. The results for the LTE model agree well with those in SOI14, the differences being due to the updated chemical network. Below, we describe the time (or, equivalently, density) evolution of the cloud with particular attention to the H_2^+ vibrational level population.

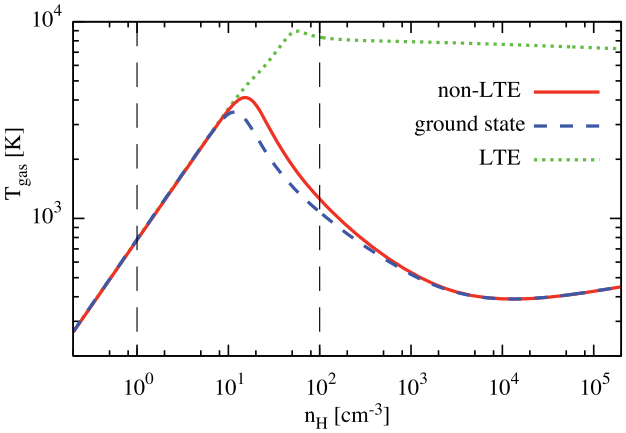

Figure 2. Temperature evolution in a collapsing primordial gas cloud irradiated by a diluted blackbody radiation with $T_{rad} = 6000$ K and $J_{21} = 0.05$ as a function of the cloud density: non-LTE model (solid red), ground-state model (dashed blue) and LTE (dotted green). The vertical lines (long-dashed black) demarcate boundaries between the low, intermediate and high-density regimes.

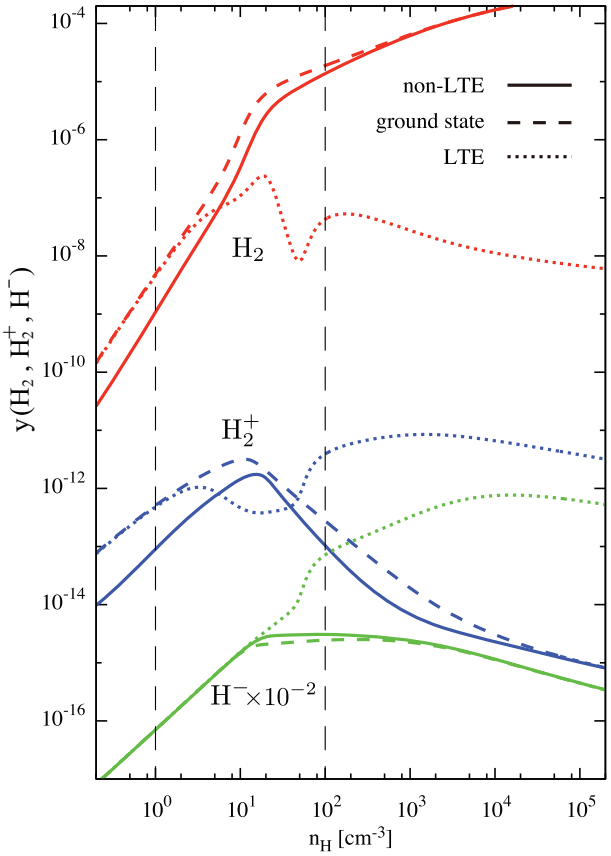

Figure 3. Abundances of H_2 (red), H_2^+ (blue) and H^- ($\times10^{-2}$; green) for the same cases as Fig. 2: non-LTE model (solid), ground-state model (dashed), and LTE (dotted) models.

3.1.1 *Low-density Regime: $n_H \lesssim 1$ cm^{-3}*

In this density range, the temperature is still very low, $T_{gas} \lesssim 10^3$ K, although it rises with density by adiabatic compression, as seen in Fig. 2. Thus, almost all H_2^+ is in the ground vibrational state if LTE is assumed (Fig. 4). However, in the non-LTE model a finite amount

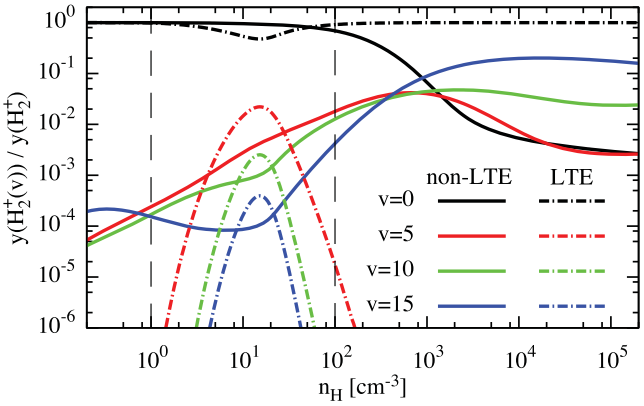

Figure 4. Populations of H_2^+ in the $v = 0$, 5, 10 and 15 vibrational levels (black, red, green and blue, respectively) in the non-LTE model (solid) for the same case as Fig. 2. The LTE populations (dot dashed) with the temperature given by T_{gas} in the non-LTE model, i.e. the solid red curve in Fig. 2, are also plotted.

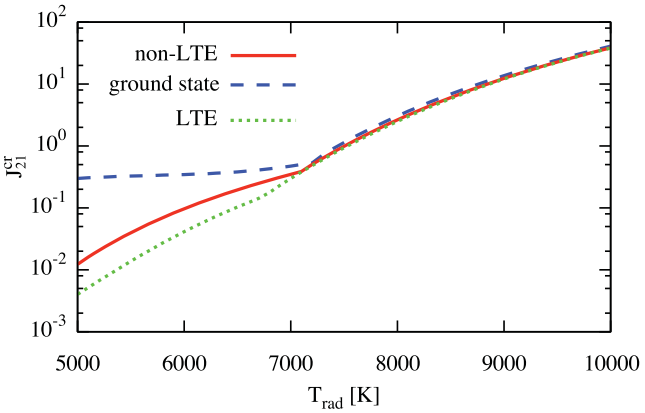

Figure 5. Critical intensity for the direct collapse J_{21}^{cr} as a function of the blackbody temperature T_{rad} of the irradiation radiation. In addition to the value in the non-LTE model (solid red), those in the ground-state (dashed blue) and LTE (dotted green) models are plotted.

of H_2^+ is in higher vibrational levels because the H_2^+ molecules tend to be formed by radiative association in excited states (reaction 4; Ramaker & Peek 1976; Babb 2015). This effect is more pronounced at low temperatures where the $v = 15$ level is more populated than the $v = 5$ and 10 levels. Note that not all the H_2^+ settles to the ground state even though the collisional excitation/de-excitation rate is much smaller than the radiative de-excitation rate in this low-density regime. This is because not only radiative de-excitation, but also radiative association and H_2^+ photodissociation contribute to the H_2^+ level population. In the non-LTE model, since a fraction of H_2^+ is in high vibrational levels, the larger H_2^+ photodissociation reaction rate results in a smaller H_2^+ abundance than in the LTE or ground-state models (Fig. 3). As a result, the amount of H_2 formed is smaller in the non-LTE case. However, in this density range, the H_2 abundance is very low, $y(H_2) \sim 10^{-9}$, in all models and does not affect the thermal evolution.

3.1.2 Intermediate-density Regime: $n_H \sim 1$–10^2 cm^{-3}

In this density regime, the evolutionary paths bifurcate into those of atomic and H_2 cooling depending on the assumed level population (Fig. 2). As seen in Fig. 4, at high temperature (∼4000 K), in the LTE approximation the excited levels are somewhat populated around ∼10 cm^{-3}. However, in the non-LTE treatment only a smaller amount of H_2^+ resides in excited states, because of the higher photodissociation rate from those levels. In LTE, the fractional abundance of excited levels, and thus the H_2^+ photodissociation rate are overestimated. This results in smaller amounts of both H_2^+ and H_2, compared to the non-LTE model (Fig. 3). Due to the lower H_2 fraction of the LTE case, the cloud collapses along the atomic cooling track, whereas in non-LTE it follows the molecular hydrogen cooling path (Fig. 2). Finally, in the ground-state model, the smaller H_2^+ photodissociation rate and the consequent larger amount of H_2 (Fig. 3) cause an earlier onset of H_2 cooling relative to the non-LTE case (Fig. 2).

3.1.3 High-density regime: $n_H \gtrsim 10^2$ cm^{-3}

The different evolutionary paths found in the previous regime are not modified at higher densities by the details of the various chemical processes. Considering the large temperature difference between LTE and the other models, it is not possible to distinguish between the effects of the level population and those related to the chemical abundances shown in Fig. 3. In this regime, unlike the LTE population, the excited levels are more populated than the ground state, as seen in Fig. 4. The reason is as follows: due to the high density, the H_2^+ photodissociation is negligible compared to collisional processes, such as radiative association, charge transfer and collisional excitation/de-excitation. Since not only collisional excitation/de-excitation, but also radiative association and charge transfer continue to play important roles, the level population does not converge to the LTE value. This effect can be considered as a pumping mechanism that depletes the ground level and allows for the occupation of higher excited states.

3.2 The critical LW intensity J_{21}^{cr}

Fig. 5 shows the critical LW intensity J_{21}^{cr} for the blackbody spectra with temperature T_{rad}. We find J_{21}^{cr} by using the bisection method, in which we examine whether the given J_{21} is high enough for the cloud to collapse along the atomic-cooling track by totally suppressing H_2 cooling (for more details, see, e.g. SOI14 and references therein). In addition to our fiducial result for the non-LTE model, those for the ground-state and LTE models are also plotted in Fig. 5 for comparison.

Two features in Fig. 5 should be noted. First, the slope of J_{21}^{cr} changes discontinuously around $T_{rad} \sim 7000$ K, accompanying the shift of dominant H_2-formation reaction determining J_{21}^{cr} from the H_2^+ channel ($T_{rad} \lesssim 7000$ K) to the H^- channel ($T_{rad} \gtrsim 7000$ K). We will discuss the condition for the H_2^+ channel to be dominant in Section 3.3. Secondly, in the range $T_{rad} \lesssim 7000$ K, J_{21}^{cr} depends on the assumed H_2^+ vibrational populations. Therefore, it is necessary to take into account the non-LTE H_2^+ level population to obtain J_{21}^{cr} correctly because the efficiency of the H_2^+ channel, the dominant H_2 formation channel in this range, is sensitive to its vibrational level population. Compared to the correct J_{21}^{cr} by the non-LTE modelling, those for the ground-state and LTE models are smaller or larger, respectively. This is because in the ground-state model (the LTE model), compared to the non-LTE model, the H_2^+ photodissociation rate is lower (higher) around the density where the bifurcation into the two evolutionary paths occurs, and thus more (less) J_{21} is needed to suppress the H_2 cooling.

On the other hand, $J_{21}^{\rm cr}$ for $T_{\rm rad} \gtrsim 7000$ K is insensitive to the H_2^+ level population because the H^- channel rather than the H_2^+ channel is important in this range to determine $J_{21}^{\rm cr}$. Recall that typical high-z galaxies have hard spectra corresponding to a blackbody with $T_{\rm rad} \gtrsim 2 \times 10^4$ K (SOI14), as mentioned in Section 2.1. Thus, our adoption of the LTE H_2^+ photodissociation rate in SOI14 to obtain $J_{21}^{\rm cr}$ for realistic spectra is justified. We plot $J_{21}^{\rm cr}$ only for $T_{\rm rad} < 10^4$ K in Fig. 5, because $J_{21}^{\rm cr}$ does not depend on the vibrational populations for $T_{\rm rad} > 10^4$ K. For $J_{21}^{\rm cr}$ in the range $T_{\rm rad} > 10^4$ K, we refer readers to, e.g. fig. 3 of SOI14.

3.3 Condition for the H_2^+-channel dominance

Here, we discuss the condition that the H_2^+ channel dominates over the H^- channel. We introduce $J_{21}^{\rm eq}$, the threshold value of J_{21} above which the H_2^+ channel is more effective in H_2 formation than the H^- channel.

To begin with, we estimate the H_2 formation rate via the H^- channel. The H^- fraction is determined by the balance between the radiative attachment (reaction 1), associative detachment (reaction 2) and photodetachment (reaction 5) as

$$y(\mathrm{H}^-) = \frac{k_{\rm ra}^{\mathrm{H}^-}\, y(\mathrm{e})}{k_{\rm ad}^{\mathrm{H}^-} + k_{\rm pd}^{\mathrm{H}^-}/n(\mathrm{H})}\,. \tag{10}$$

The H_2 formation rate via the H^- channel is given by

$$\begin{aligned}\frac{\mathrm{d}y_{\mathrm{H}_2}^{\mathrm{H}^-}}{\mathrm{d}t} &= k_{\rm ad}^{\mathrm{H}^-}\, y(\mathrm{H}^-)\, n(\mathrm{H}) \\ &\simeq \frac{k_{\rm ra}^{\mathrm{H}^-}\, y(\mathrm{e})\, n(\mathrm{H})}{1 + k_{\rm pd}^{\mathrm{H}^-}/\left(n(\mathrm{H})\, k_{\rm ad}^{\mathrm{H}^-}\right)}\,,\end{aligned} \tag{11}$$

where we have used equation (10) in the second line. Similarly, we estimate the H_2 formation rate via the H_2^+ channel. The H_2^+ fraction is determined by the balance between radiative association (reaction 3), charge transfer (reaction 4) and photodissociation (reaction 6) as

$$y(\mathrm{H}_2^+) = \frac{k_{\rm ra}^{\mathrm{H}_2^+}\, y(\mathrm{H}^+)}{k_{\rm ct}^{\mathrm{H}_2^+} + k_{\rm pd}^{\mathrm{H}_2^+}/n(\mathrm{H})}\,. \tag{12}$$

The H_2 formation rate via the H_2^+ channel, i.e. the charge transfer rate, is given by

$$\begin{aligned}\frac{\mathrm{d}y_{\mathrm{H}_2}^{\mathrm{H}_2^+}}{\mathrm{d}t} &= k_{\rm ct}^{\mathrm{H}_2^+}\, y(\mathrm{H}_2^+)\, n(\mathrm{H}) \\ &\simeq \frac{k_{\rm ra}^{\mathrm{H}_2^+}\, y(\mathrm{H}^+)\, n(\mathrm{H})}{1 + k_{\rm pd}^{\mathrm{H}_2^+}/\left(n(\mathrm{H})\, k_{\rm ct}^{\mathrm{H}_2^+}\right)}\,,\end{aligned} \tag{13}$$

where we have used equation (12) in the second line. By equating equations (11) and (13), we obtain

$$J_{21}^{\rm eq} \simeq \left(\frac{k_{\rm ra}^{\mathrm{H}^-}}{k_{\rm ra}^{\mathrm{H}_2^+}} - 1\right) \frac{k_{\rm ad}^{\mathrm{H}^-}\, n_{\rm H}}{k_{\rm pd}^{\mathrm{H}^-}|_{J_{21}=1}}\,, \tag{14}$$

where we have used $k_{\rm pd}^{\mathrm{H}^-} = k_{\rm pd}^{\mathrm{H}^-}|_{J_{21}=1} \times J_{21}$, $n(\mathrm{H}) \simeq n_{\rm H}$ and $y(\mathrm{e}) \simeq y(\mathrm{H}^+)$ and neglected $k_{\rm pd}^{\mathrm{H}_2^+}$ for simplicity. The effect of H_2^+ photodissociation would substantially change the expression given by equation (14) if the LTE rate was used. However, the actual rate of H_2^+ photodissociation just before the atomic- and H_2-cooling tracks bifurcate is lower than the LTE one, as shown in Section 3.1.2. Thus, the correction due to H_2^+ photodissociation makes $J_{21}^{\rm eq}$ given by equation (14) larger at most by a factor of a few and can be neglected in the order-of-magnitude estimate here.

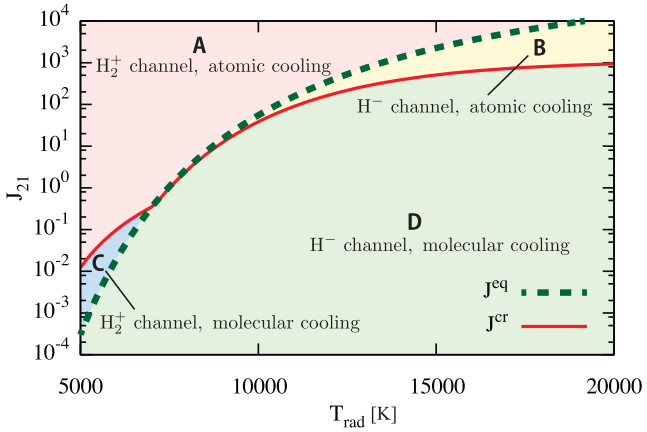

Figure 6. The threshold value $J_{21}^{\rm eq}$ (dashed green), given by equation (14), above which the H_2^+ channel is more effective than the H^- channel at $n_{\rm H} = 10^2\,{\rm cm}^{-3}$. The critical intensity $J_{21}^{\rm cr}$ for the direct collapse shown in Fig. 5 (solid red) is overplotted. The explanation for the domains A–D is given in the text.

To evaluate $J_{21}^{\rm eq}$, we consider the physical condition of the gas just before the atomic- and H_2-cooling tracks bifurcate (see, e.g. Omukai 2001 or SOI14) and take $T_{\rm gas} = 8000$ K and $n_{\rm H} = 10^2\,{\rm cm}^{-3}$. The density $n_{\rm H}$ at bifurcation depends on the spectra and it is closer to $10^2\,{\rm cm}^{-3}$ for soft spectra with $T_{\rm rad} \lesssim 10^4$ K, which is of our interest in this paper, although it is about $10^3\,{\rm cm}^{-3}$ for $T_{\rm rad} \sim 10^5$ K. The reaction rate coefficients at 8000 K are given by $k_{\rm ra}^{\mathrm{H}^-} \approx 6 \times 10^{-15}\,{\rm cm}^3\,{\rm s}^{-1}$, $k_{\rm ad}^{\mathrm{H}^-} \approx 9 \times 10^{-10}\,{\rm cm}^3\,{\rm s}^{-1}$ and $k_{\rm ra}^{\mathrm{H}_2^+} \simeq 1.5 \times 10^{-16}\,{\rm cm}^3\,{\rm s}^{-1}$ (GP98) and the H^- photodetachment rate is given by Fig. 1. By substituting the above reaction rate coefficients and photodetachment rate into equation (14), we obtain $J_{21}^{\rm eq}$, as shown in Fig. 6. Also shown is $J_{21}^{\rm cr}$ obtained in Section 3.2 for comparison. Depending on the value of J_{21} relative to $J_{21}^{\rm cr}$ and $J_{21}^{\rm eq}$, the way in which a cloud evolves falls within one of the following four cases (Fig. 6):

A: $J_{21} > J_{21}^{\rm cr}$ and $J_{21} > J_{21}^{\rm eq}$. The cloud collapses along the atomic-cooling track, since H_2, formed mainly via the H_2^+ channel, is not enough to cool the gas.

B: $J_{21} > J_{21}^{\rm cr}$ and $J_{21} < J_{21}^{\rm eq}$. The cloud collapses along the atomic-cooling track, since H_2, formed mainly via the H^- channel, is not enough to cool the gas.

C: $J_{21} < J_{21}^{\rm cr}$ and $J_{21} > J_{21}^{\rm eq}$. The cloud collapses along the H_2-cooling track due to H_2 formation mainly via the H_2^+ channel.

D: $J_{21} < J_{21}^{\rm cr}$ and $J_{21} < J_{21}^{\rm eq}$. The cloud collapses along the H_2-cooling track due to H_2 formation mainly via the H^- channel.

In the soft-spectrum regime of $T_{\rm rad} \lesssim 7000$ K, where $J_{21}^{\rm eq} \lesssim J_{21}^{\rm cr}$, the cases A, C and D can be realized depending on J_{21}. In the case C, in particular, while the H^- channel is blocked by radiation, sufficient H_2 for cooling can still form via the H_2^+ channel. In this case, the proper account of the H_2^+ level population is indispensable since the H_2 formation rate via the H_2^+ channel is sensitive to its level population, as shown by the example in Section 3.1. On the other hand, in the hard-spectrum regime of $T_{\rm rad} \gtrsim 7000$ K, where $J_{21}^{\rm cr} \lesssim J_{21}^{\rm eq}$, the cases A, B and D are allowed, there is no range of J_{21} satisfying $J_{21}^{\rm eq} < J_{21} < J_{21}^{\rm cr}$. Namely, radiation fields strong enough to block the H^- channel always exceed the critical intensity to totally suppress H_2 formation by H_2 photodissociation. This means

that the H_2-cooling track cannot be realized by the H_2^+ channel for $T_{\rm rad} \gtrsim 7000$ K.

4 DISCUSSION AND CONCLUSIONS

We have computed the thermal and chemical evolution of primordial gas clouds resolving the vibrational levels of H_2^+, which enables us to properly implement H_2 formation via the H_2^+ channel. The efficiency of H_2^+ photodissociation, which suppresses the H_2^+ channel by destroying the intermediate product H_2^+, is sensitive to the level population of the molecular ion. We have found that H_2 formation via the H_2^+ channel becomes more effective in the non-LTE model than in LTE because more H_2^+ is in the ground state and thus its photodissociation rate is smaller.

As to the effects of the background radiation, we have found that H_2 formation via the H_2^+ channel becomes important in clouds irradiated by strong radiation fields with soft spectra characterized by $T_{\rm rad} \lesssim 7000$ K. In this case, the cloud thermal evolution is strongly affected by the H_2^+ level population, indicating the importance of non-LTE treatment of the H_2^+ vibrational levels. On the other hand, under radiation fields with harder spectra and $T_{\rm rad} \gtrsim 7000$ K, the H_2^+ channel always falls short of the H^- channel in producing H_2 molecules.

We have derived the critical radiation intensity $J_{21}^{\rm cr}$ for the formation of SMS by direct collapse and examined its dependence on the assumed H_2^+ level population. For soft spectra with $T_{\rm rad} \lesssim 7000$ K, the critical intensity $J_{21}^{\rm cr}$ is under(over)-estimated if the level population is assumed to be in LTE (if all the H_2^+ is assumed to be in the ground state). On the other hand, the value of $J_{21}^{\rm cr}$ is independent of the assumed H_2^+ level population for harder spectra with $T_{\rm rad} \gtrsim 7000$ K. Therefore, since typical high-redshift radiation sources, i.e. young and/or metal-poor galaxies, have rather hard spectra corresponding to blackbodies with $T_{\rm rad} \gtrsim 2 \times 10^4$ K (SOI14), the LTE approximation adopted in SOI14 in determining $J_{21}^{\rm cr}$ for realistic spectra is justified.

We note that primordial gas clouds may be exposed to much softer radiation fields. For example, galaxies with extremely strong Ly α emission can be regarded as characterized by very soft spectra. Since the energy of Ly α photons ($h\nu = 10.2$ eV) is below the lower limit of the LW bands ($h\nu = 11.2$–13.6 eV), such emission would only destroy H^- leaving H_2 unaffected. Also, since the initial mass function in high-redshift galaxies is poorly constrained, the infrared/optical cosmic background radiation originating from these sources can be soft with temperature $T_{\rm rad} \sim 6000$ K, corresponding to the typical stellar mass $\sim 0.7\ {\rm M}_\odot$, as considered in Wolcott-Green & Haiman (2012).

In non-standard cosmology, primordial density fluctuations are expected to be enhanced at small scales, so that the first stellar objects can form at very early times with $z \gtrsim 100$, as considered in Hirano et al. (2015). Under the strong and very soft CMB radiation at that time ($T_{\rm rad} \gtrsim 300$ K), H_2 formation via the H_2^+ channel can be the dominant path with the H^- channel blocked by radiation processes (including non-thermal photons that play an additional role in enhancing H^- photodetachment; Coppola et al. 2013).

As a last example, let us consider the case where direct collapse via the atomic-cooling track is realized. In such a case, the growing protostar results in a very extended structure with radius $R \simeq 30$ au ('supergiant' protostar) and low effective temperature $T_{\rm rad} \simeq 5000$ K (Hosokawa et al. 2012, 2013). In studying the physical conditions in the region around the supergiant protostar, the non-LTE H_2^+ level population must be taken into account.

In this paper, the collapse of primordial gas clouds has been calculated by resolving the H_2^+ vibrational levels, to our knowledge, for the first time. However, neither H_2^+ rotational levels nor H_2 rovibrational levels have been explicitly included. Although the H_2^+ rotationally resolved kinetics is probably not important, the H_2 rovibrationally resolved kinetics may have considerable effects. The H_2 rovibrational level population affects critical processes in the evolution of the primordial gas, such as photodissociation, collisional dissociation and cooling by molecular hydrogen. We plan to include the full level-resolved kinetics of H_2 and H_2^+ in future studies.

ACKNOWLEDGEMENTS

KS would like to thank D. Nakauchi, H. Yajima and K. Toma for fruitful discussions and valuable comments. KS would also like to thank Savino Longo and University of Bari for hospitality and support during his visit to University of Bari. This work is supported in part by MEXT/JSPS KAKENHI Grant Number 15J03873 (KS) and 25287040 (KO). The authors acknowledge the discussions within the international team #272 lead by C. M. Coppola 'EUROPA - Early Universe: Research on Plasma Astrochemistry' at ISSI (International Space Science Institute) in Bern.

REFERENCES

Agarwal B., Khochfar S., 2015, MNRAS, 446, 160
Agarwal B., Khochfar S., Johnson J. L., Neistein E., Dalla Vecchia C., Livio M., 2012, MNRAS, 425, 2854
Anninos P., Zhang Y., Abel T., Norman M. L., 1997, New Astron., 2, 209
Babb J. F., 2015, ApJS, 216, 21
Becerra F., Greif T. H., Springel V., Hernquist L. E., 2015, MNRAS, 446, 2380
Bromm V., Loeb A., 2003, ApJ, 596, 34
Choi J.-H., Shlosman I., Begelman M. C., 2015, MNRAS, 450, 4411
Coppola C. M., Longo S., Capitelli M., Palla F., Galli D., 2011, ApJS, 193, 7 (C11)
Coppola C. M., Galli D., Palla F., Longo S., Chluba J., 2013, MNRAS, 434, 114
Dijkstra M., Haiman Z., Mesinger A., Wyithe J. S. B., 2008, MNRAS, 391, 1961
Dijkstra M., Ferrara A., Mesinger A., 2014, MNRAS, 442, 2036
Draine B. T., Bertoldi F., 1996, ApJ, 468, 269
Dunn G. H., 1968, Phys. Rev., 172, 1
Fan X. et al., 2001, AJ, 122, 2833
Galli D., Palla F., 1998, A&A, 335, 403 (GP98)
Gealy M. W., van Zyl B., 1987, Phys. Rev. A, 36, 3100
Glover S., 2015a, MNRAS, 451, 2082
Glover S. C. O., 2015b, MNRAS, 453, 2901
Glover S. C. O., Abel T., 2008, MNRAS, 388, 1627
Hartwig T., Glover S. C. O., Klessen R. S., Latif M. A., Volonteri M., 2015, MNRAS, 452, 1233
Hirano S., Zhu N., Yoshida N., Spergel D., Yorke H. W., 2015, ApJ, 814, 18
Hirata C. M., Padmanabhan N., 2006, MNRAS, 372, 1175
Hosokawa T., Omukai K., Yoshida N., Yorke H. W., 2011, Science, 334, 1250
Hosokawa T., Omukai K., Yorke H. W., 2012, ApJ, 756, 93
Hosokawa T., Yorke H. W., Inayoshi K., Omukai K., Yoshida N., 2013, ApJ, 778, 178
Inayoshi K., Tanaka T. L., 2015, MNRAS, 450, 4350
Inayoshi K., Omukai K., Tasker E., 2014, MNRAS, 445, L109
John T. L., 1988, A&A, 193, 189
Krstić P. S., 2005, Nucl. Instrum. Methods Phys. Res. B, 241, 58
Krstić P. S., Janev R. K., 2003, Phys. Rev. A, 67, 022708
Krstić P. S., Schultz D. R., 1999, J. Phys. B: At. Mol. Opt. Phys., 32, 2415
Krstić P. S., Schultz D. R., Janev R. K., 2002, Phys. Scr. T, 96, 61

Larson R. B., 1969, MNRAS, 145, 271
Latif M. A., Bovino S., Van Borm C., Grassi T., Schleicher D. R. G., Spaans M., 2014, MNRAS, 443, 1979
Lenzuni P., Chernoff D. F., Salpeter E. E., 1991, ApJS, 76, 759
Longo S., Coppola C. M., Galli D., Palla F., Capitelli M., 2011, Rend. Fis. Acc. Lincei, 22, 119
McGreer I. D., Bryan G. L., 2008, ApJ, 685, 8
Martin P. G., Schwarz D. H., Mandy M. E., 1996, ApJ, 461, 265
Mihajlov A. A., Ignjatović L. M., Sakan N. M., Dimitrijević M. S., 2007, A&A, 469, 749
Miyake S., Stancil P. C., Sadeghpour H. R., Dalgarno A., McLaughlin B. M., Forrey R. C., 2010, ApJ, 709, L168
Mortlock D. J. et al., 2011, Nature, 474, 616
Nagakura T., Omukai K., 2005, MNRAS, 364, 1378
Nakauchi D., Inayoshi K., Omukai K., 2014, MNRAS, 442, 2667
Olivares Pilón H., Baye D., 2012, J. Phys. B: At. Mol. Opt. Phys., 45, 065101
Omukai K., 2001, ApJ, 546, 635
Omukai K., Schneider R., Haiman Z., 2008, ApJ, 686, 801
Penston M. V., 1969, MNRAS, 144, 425
Posen A. G., Dalgarno A., Peek J. M., 1983, At. Data Nucl. Data Tables, 28, 265
Ramaker D. E., Peek J. M., 1976, Phys. Rev. A, 13, 58
Regan J. A., Haehnelt M. G., 2009a, MNRAS, 393, 858
Regan J. A., Haehnelt M. G., 2009b, MNRAS, 396, 343
Regan J. A., Johansson P. H., Haehnelt M. G., 2014a, MNRAS, 439, 1160
Regan J. A., Johansson P. H., Wise J. H., 2014b, ApJ, 795, 137
Richings A. J., Schaye J., Oppenheimer B. D., 2014, MNRAS, 442, 2780
Sakurai Y., Hosokawa T., Yoshida N., Yorke H. W., 2015, MNRAS, 452, 755
Shang C., Bryan G. L., Haiman Z., 2010, MNRAS, 402, 1249
Shapiro S. L., Teukolsky S. A., 1983, Black Holes, White Dwarfs, and Neutron Stars: The Physics of Compact Objects, Wiley, New York
Shlosman I., Choi J.-H., Begelman M. C., Nagamine K., 2015, preprint (arXiv:1508.05098v1)
Stancil P. C., 1994, ApJ, 430, 360
Sugimura K., Omukai K., Inoue A. K., 2014, MNRAS, 445, 544 (SOI14)
van Zyl B., Le T. Q., Amme R. C., 1981, J. Chem. Phys., 74, 314
Venemans B. P. et al., 2013, ApJ, 779, 24
Wishart A. W., 1979, MNRAS, 187, 59
Wolcott-Green J., Haiman Z., 2011, MNRAS, 412, 2603
Wolcott-Green J., Haiman Z., 2012, MNRAS, 425, L51
Wolcott-Green J., Haiman Z., Bryan G. L., 2011, MNRAS, 418, 838
Wu X.-B. et al., 2015, Nature, 518, 512
Yahil A., 1983, ApJ, 265, 1047
Yoshida N., Omukai K., Hernquist L., 2008, Science, 321, 669

APPENDIX A: H_2^+ ROTATIONAL LEVEL POPULATION

Here, we describe our treatment of the H_2^+ rotational level populations. Since comprehensive rotational-state-resolved data is not available in the literature, we use the interpolation formula by Glover (2015a). Specifically, we calculate the H_2^+ photodissociation rate from each vibrational level by the formula $k = k_{\rm LTE}\,(k_{\rm n\to 0}/k_{\rm LTE})^{\alpha}$, where $k_{\rm n\to 0}$ and $k_{\rm LTE}$ are the rates for the ground rotational state and the LTE rotational level population, respectively, $\alpha = (1 + n_{\rm H}/n_{\rm cr})^{-1}$ and $n_{\rm cr}$ is the critical density for the LTE populations, which is $\sim 10^3\,{\rm cm}^{-3}$ for $T_{\rm gas} = 8000\,{\rm K}$ (Glover 2015a).

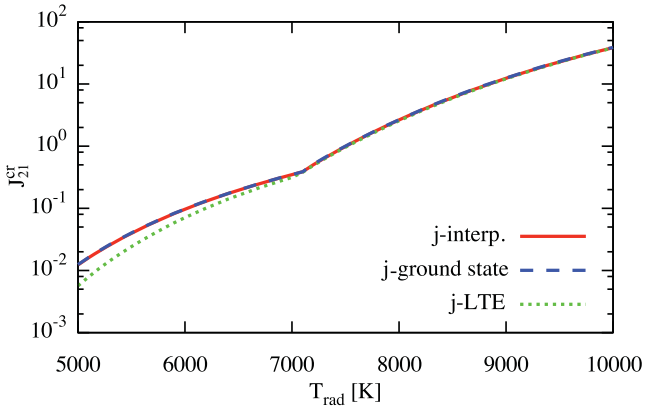

Figure A1. Same as Fig. 5, but for three different assumptions on the H_2^+ rotational level population: (i) model using the interpolation formula by Glover (2015a), (ii) model where all the H_2^+ in each vibrational level is in its rotational ground state and (iii) model assuming the rotational LTE. Note that the H_2^+ vibrational levels are resolved in all the cases.

To estimate the error in our modelling of the H_2^+ rotational level population, we compare the critical intensity $J_{21}^{\rm cr}$ obtained with three different modelling of rotational level population: (i) the fiducial *j*-interp. model based on Glover (2015a); (ii) the *j*-ground state model assuming that all the H_2^+ in each vibrational level resides in the ground rotational state; and (iii) the *j*-LTE model assuming the LTE rotational level population in each vibrational level. Fig. A1 shows that the values of $J_{21}^{\rm cr}$ in the *j*-interp. and *j*-ground state models are almost identical while in the *j*-LTE model it is slightly smaller. This difference is, however, much smaller than that among the vibrationally non-LTE and LTE models shown in Fig. 5, indicating that the cloud thermal evolution does not depend so much on rotational level population as the vibrational level population.

This paper has been typeset from a TEX/LATEX file prepared by the author.